A Simple Model to Estimate Plantarflexor Muscle–Tendon Mechanics and Energetics During Walking With Elastic Ankle Exoskeletons

Gregory S. Sawicki* and Nabil S. Khan

Abstract*—*Goal:* A recent experiment demonstrated that when humans wear unpowered elastic ankle exoskeletons with intermediate spring stiffness, they can reduce their metabolic energy cost to walk by ∼7%. Springs that are too compliant or too stiff have little benefit. The purpose of this study was to use modeling and simulation to explore the muscle-level mechanisms for the "sweet spot" in stiffness during exoskeleton assisted walking.** ***Methods: **We developed a simple lumped uniarticular musculoskeletal model of the plantarflexors operating in parallel with an elastic "exo-tendon." Using an inverse approach with constrained kinematics and kinetics, we rapidly simulated human walking over a range of exoskeleton stiffness values and examined the underlying neuromechanics and energetics of the biological plantarflexors.** ***Results:*** **Stiffer ankle exoskeleton springs resulted in larger decreases in plantarflexor muscle forces, activations, and metabolic energy consumption. However, in the process of unloading the compliant biological muscle–tendon unit, the muscle fascicles experienced larger excursions that negatively impacted series elastic element recoil that is characteristic of a tuned "catapult mechanism."** ***Conclusion:*** **The combination of disrupted muscle–tendon dynamics and the need to produce compensatory forces/moments to maintain overall net ankle moment invariance could explain the "sweet spot" in metabolic performance at intermediate ankle exoskeleton stiffness. Future work will aim to provide experimental evidence to support the model predictions presented here using ultrasound imaging of muscle-level dynamics during walking with elastic ankle exoskeletons.** ***Significance:*** **Engineers must account for the muscle-level effects of exoskeleton designs in order to achieve maximal performance objectives.**

***Index Terms*—Ankle exoskeleton, computer simulation, elastic energy storage, energetics, Hill-type muscle model, human walking, metabolic cost, muscle–tendon dynamics, plantarflexors (PF).**

I. Introduction

HUMAN walking [4], hopping [5], and running [6] all exhibit compliant dynamics that can be captured by simple spring–mass models. In essence, the lower limb is able to compress and recoil elastically with stiffness that arises from the combination of passive nonlinear material properties of the muscles and series elastic connective tissues, and active neuromuscular control. During locomotion, "springy limbs" enable a number of elastic mechanisms that are exploited to improve performance. For example, properly timed stretch and recoil of series elastic tissues can be used to enhance muscle power output during acceleration, attenuate muscle power requirements during deceleration, or conserve mechanical and metabolic energy during steady-speed locomotion [7].

The range of performance benefits afforded by compliant limbs in humans and animals has inspired wearable exoskeletons (EXOs) that may have applications in both gait rehabilitation and augmentation. Recently, a number of lower limb EXOs have been developed that use elastic elements (i.e., springs and clutches) in parallel with the limb to strategically store and return energy and help power locomotion [8]–[15]. Physiological measurements in studies of vertical hopping in elastic EXOs spanning the whole limb [9], the knee joint [14] and the ankle joint [10], [12], [20] indicate performance benefits that include reduced muscle activity, reduced biological limb/joint stiffness and mechanical power output, and reduced metabolic energy cost of the user. These studies of simple movements like vertical hopping have paved the way for the continued development and implementation of elastic EXOs to improve user performance during human walking and running gaits.

During human walking, the majority of mechanical power comes from the ankle plantarflexors (PFs) [21]. Furthermore, approximately half of the requisite mechanical power output at the ankle comes from elastic recoil of the Achilles' tendon at "push off" [22]. Given the PFs' primary role in forward propulsion [23] and the significant elastic mechanism afforded by their compliant muscle–tendon architecture, the ankle joint seems to be a logical site for a passive elastic EXO that can improve human walking performance.

We have recently developed a novel passive elastic ankle EXO that can store and return energy during the stance phase while allowing free ankle rotation during the swing phase of walking [8], [24], [25]. The key feature in the design is a rotary clutch that uses a ratchet and pawl configuration and two timing pins set to engage and disengage the EXO spring at set ankle joint angles. The EXO spring is engaged when the first timing pin pushes the pawl onto the ratchet at terminal swing, where the ankle dorsiflexes just prior to heel strike. This enables the spring to store and return elastic energy during stance. Then, once the ankle reaches extreme plantarflexion, after the foot is off the

Manuscript received March 6, 2015; revised August 17, 2015; accepted September 18, 2015. Date of publication October 15, 2015; date of current version May 19, 2016. The work of G. S. Sawicki was supported by the US-Israel Binational Science Foundation under Grant #2011152 and the National Institute of Nursing Research of the National Institutes of Health under Grant #R01NR014756. *Asterisk indicates corresponding author.*

*G. S. Sawicki is with the Joint Department of Biomedical Engineering, North Carolina State University and the University of North Carolina-Chapel Hill, Raleigh, NC 27695 USA (e-mail: greg_sawicki@ncsu.edu).

N. S. Khan is with Anuva Innovations, Inc.

This paper has supplementary downloadable material available at http://ieeexplore.ieee.org (File size: 1 MB).

Color versions of one or more of the figures in this paper are available online at http://ieeexplore.ieee.org.

Digital Object Identifier 10.1109/TBME.2015.2491224

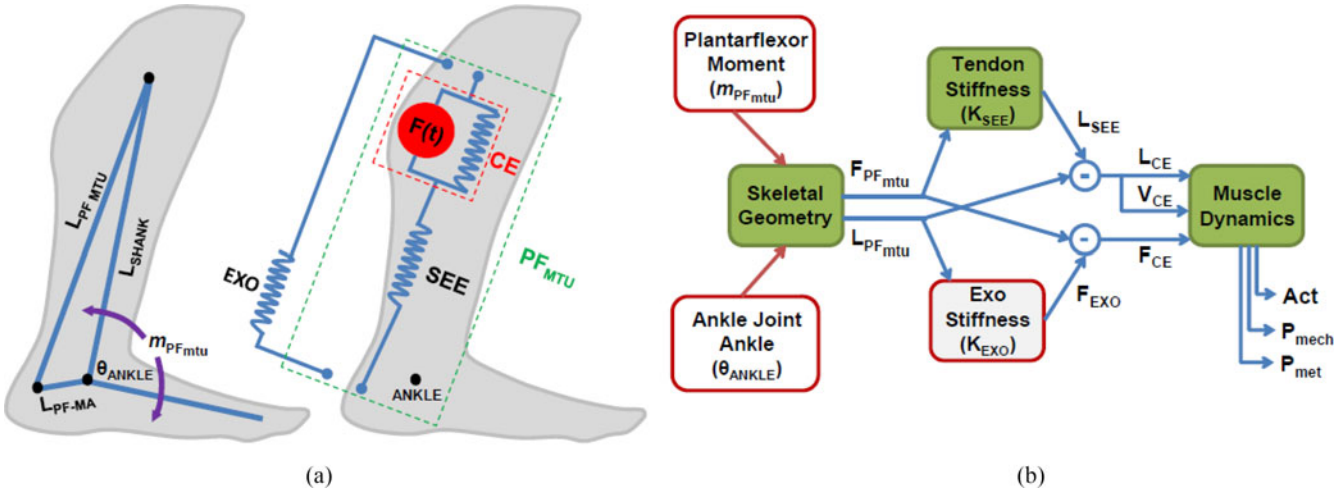

Fig. 1. (a) Modeling schematic. We modeled the combined triceps surae (soleus and gastrocnemius muscles) as a single lumped uniarticular PF ($\mathrm{PF}_{\mathrm{mtu}}$) attached along the shank L_{SHANK} to the calcaneus with length $L_{\mathrm{PF}_{\mathrm{mtu}}}$ and moment arm $L_{\mathrm{PF}-MA}$ (left). The lumped $\mathrm{PF}_{\mathrm{mtu}}$ generated force according to a Hill-type muscle–tendon model with a muscle CE comprising active ($F(t)$, red) and passive (blue parallel spring) components and a series elastic component (SEE) representing the Achilles' tendon and aponeurosis. We modeled a passive elastic ankle EXO as a spring in parallel with the $\mathrm{PF}_{\mathrm{MTU}}$ and acting through the same moment arm $L_{\mathrm{PF}-MA}$ (right). (b) Block diagram of computational flow in the inverse modeling framework used to simulate changes in muscle-level dynamics during walking with EXOs of varying spring stiffness K_{EXO}. First, using the defined skeletal geometry, the PF moment $m_{\mathrm{PF}_{\mathrm{mtu}}}$ and ankle joint angle θ_{ANKLE} from normal walking at 1.25 m/s were converted to a PF force, $F_{\mathrm{PF}_{\mathrm{mtu}}}$ and PF length, $L_{\mathrm{PF}_{\mathrm{mtu}}}$, respectively. Then, we used the SEE stiffness, K_{SEE} to compute SEE length, L_{SEE}; and the EXO stiffness, K_{EXO} to compute EXO force, F_{EXO}. Next, we could use subtraction to define the force (F_{CE}), length (L_{CE}), and velocity (V_{CE}), of the muscle. Finally, these values were used along with models of muscle force production and metabolic energy use to compute muscle activation (Act), mechanical power output (P_{mech}) and metabolic power output (P_{met}).

ground, a second timing pin pushes the pawl off of the ratchet, allowing the user to freely rotate their foot without interference from the EXO spring. This EXO design is simple, lightweight (<500 g), and requires no electronics or battery, making it a low-cost option for gait assistance. We have recently shown that users can use this unpowered EXO to reduce their metabolic cost of walking by ∼7% below normal walking, but only when the EXO spring (i.e., "exo-tendon") is not too compliant and not too stiff [25]. The reasons behind the existence of a "sweet spot" for ankle EXO stiffness remain unresolved, principally because it is difficult to experimentally observe the muscle-level effects of EXO mechanical assistance.

The goal of this study was to develop and employ a simple *in silico* modeling tool to aid in the muscle-level understanding of the effects of increasing elastic ankle EXO stiffness on underlying PF muscle–tendon mechanics and energetics during walking. Humans tend to reduce their biological ankle moment contribution in order to maintain consistent overall ankle joint kinetics during walking with ankle EXOs [11], [25], [29], [30]. In line with this adaptive behavior, it follows that higher EXO stiffness should result in the increased unloading of biological muscle–tendons and larger reductions in the metabolic cost of plantarflexion during walking. On the other hand, if elastic ankle EXOs get *too stiff*, costly compensations might arise elsewhere in the lower limb [31] or locally at the ankle in antagonistic muscle groups (e.g., tibialis anterior) to maintain steady-gait mechanics. Furthermore, at the muscle–tendon level, increasing ankle EXO stiffness could disrupt the normal "catapult mechanism" exhibited by the ankle PFs. That is, as parallel spring stiffness increases and the EXO takes over more and more of the PF moment, the Achilles' tendon should undergo less stretch requiring larger excursions of the muscles fascicles in series. Higher muscle shortening velocities are more metabolically costly. Thus, despite lower muscle force/moment requirements, it is possible that unfavorable shifts in force–length or force–velocity operating point (e.g., higher shorting velocities) could increase metabolic energy requirements in the PF muscles and offset the potential benefit of increased assistance from elastic ankle EXOs [20], [32], [33].

To begin to resolve the reasons behind the "sweet spot" in ankle EXO stiffness, we built a strategically simple musculoskeletal model of a passive elastic ankle EXO working in parallel with the human ankle PFs [see Fig. 1(a)]. We first used experimental kinematic and kinetic data from normal walking without EXOs at 1.25 m/s to identify the best set of morphological parameters and neural activation ($\vec{M}_{\mathrm{bio}}$) that generated "human-like" ankle neuromechanics and energetics (e.g., [18]). Then with $\vec{M}_{\mathrm{bio}}$ as baseline, and an inverse framework [see Fig. 1(b)], we performed computer simulations to estimate how changes in ankle EXO stiffness in parallel with the PFs would impact the underlying biological muscle-level neuromechanics and energetics.

II. Methods

A. Model Composition

We constructed a simplified model of the human triceps surae using a single, lumped, uniarticular ankle PF muscle–tendon unit (MTU). Within the MTU, there was a Hill-type contractile element (CE), representing the muscle fascicles, and a series elastic element (SEE), representing tendonous tissues (i.e., Achilles' tendon and aponeuroses) [34] [see Fig. 1(a)]. The

extended model also included a spring in parallel with and operating through the same moment arm as the biological MTU [see Fig. 1(a)] in order to capture the dynamics of an elastic ankle EXO. More details describing mathematical relations used to model components of the MTU are provided in the online Supplementary Materials.

B. Setting Model Parameter Values

We set model parameters describing attachment geometry, MTU morphology, and muscle (CE) and tendon (SEE) force production based on the latest anatomical and physiological data from the literature (e.g., [3], [16]) as well as computer optimization (e.g., [18]) to match model outputs to baseline experimental walking data (see Table I, unbold and bold, respectively). We termed this "baseline" lumped muscle model without an EXO the $\vec{M}_{\rm bio}$ parameter configuration. More details on how we set parameters are provided in the online Supplementary Materials.

C. Extending the Model to Include an Elastic Ankle EXO

We modified the "baseline" lumped muscle model configured to $\vec{M}_{\rm bio}$ (see Table I, bold; see Supplementary Materials for more details) to include a passive elastic EXO, represented by an additional passive elastic element operating in parallel with and along the same line of action as the lumped PF MTU [see Fig. 1(a)]. In this configuration, the EXO spring (i.e., exo-tendon) operated through the same moment arm ($\sim$4.1 cm) as the PF MTU throughout the stride—a simplification that is convenient for tying the EXO back to parameters of the biological MTU (i.e., $K_{\rm SEE}$) and allows simple conversion to equivalent effective rotational stiffness values—both features that facilitate broad generalization to devices with varying geometries.

We modeled the mechanical action of EXO based on the passive ankle EXO developed by Wiggin *et al.* which utilizes a clutch to strategically engage and disengage a coil tension spring according to kinematic cues based on ankle angle [8], [24], [25]. The length of the EXO spring always exactly tracked the length of the lumped PF MTU $L_{\rm PF_{mtu}}$

$$L_{\rm EXO}(t) = L_{\rm PF_{mtu}}(t). \tag{1}$$

To model the function of the clutch, the effective slack length of the EXO spring $L_{\rm EXO_0}$ was set to the MTU length at which the ankle angle transitioned from plantarflexion into dorsiflexion shortly after heel strike

$$\begin{aligned} L_{\rm EXO_0} &= L_{\rm PF_{mtu}}(t^*) \text{ where } \frac{d\theta_{\rm ankle}}{dt}(t^*) \\ &= 0 \text{ and } \frac{d^2\theta_{\rm ankle}}{dt^2}(t^*) > 0. \end{aligned} \tag{2}$$

After this point, the EXO spring stored and released energy until the second transition from plantarflexion to dorsiflexion, at which time EXO force generation capability was terminated (i.e., shortly before swing). EXO force generation was modeled using a Hookean spring with linear stiffness $K_{\rm EXO}$

$$\begin{aligned} F_{\rm EXO}(t) &= K_{\rm EXO} \times (L_{\rm EXO}(t) - L_{\rm EXO_0}),\ L_{\rm EXO} > L_{\rm EXO_0} \\ F_{\rm EXO}(t) &= 0, \quad L_{\rm EXO} < L_{\rm EXO_0}. \end{aligned} \tag{3}$$

TABLE I
BASELINE MODEL PARAMETERS AND $\vec{\mathbf{M}}_{\mathbf{bio}}$ SOLUTION

Parameter	VALUE (UNITS) (NORM.)	Source/Details
Body Mass	70 kg	Average mass of subjects from experimental data set for walking at 1.25 m/s [2]. Within 1 SD of average subject mass from Ward *et al.* (82.7 $\pm$ 15.2 kg) [3].
Body Height	1.70 m	Average height of subjects from experimental data set for walking at 1.25 m/s [2]. Within 1 SD of average subject height from Ward *et al.* (168.4 $\pm$ 9.3 m) [3].
Shank Length, $L_{\rm SHANK}$	0.40 m	Set 0.03 m greater than tibial length from Ward *et al.* (37.1 $\pm$ 2.2 cm) [3] to include distance to femoral condyles.
$F_{\rm CE_{MAX}}$	6000 N	Similar to approximations for soleus + med. and lat. gastrocnemius muscles used by Arnold *et al.* (5500.3 N) [16] and others [17]–[19].
$V_{\rm CE_{MAX}}$	0.326 m/s (8.24 x $L_{\rm CE_0}$)	Based on values for soleus and combined gastrocnemius reported by Geyer *et al.* [19] and scaled using physiological cross section (PCSA) data from Ward *et al.* [3].
$L_{\rm CE_0}/L_{\rm PF_{mtu0}}$	0.108 (unitless)	Based on fascicle lengths for soleus, med. gastrocnemius and lat. gastrocnemius reported in Ward *et al.* [3] and tendon slack lengths reported in Arnold *et al.* [16] and scaled using physiological cross section (PCSA) data from Ward *et al.* [3]
$\boldsymbol{L_{PF_{mtu_0}}}$	**0.366 m (0.92 $\times$ $\mathbf{L_{SHANK}}$)**	
$\boldsymbol{L_{CE_0}}$	**0.040 m (0.10 $\times$ $\mathbf{L_{SHANK}}$)**	These values (in bold) were all obtained using an optimization to find the morphology that would minimize error between the modeled and measured PF moment based on inverse dynamics analysis of human walking data collected at 1.25 m/s. See text for details.
$\boldsymbol{L_{SEE_0}}$	**0.326 m (0.82 $\times$ $\mathbf{L_{SHANK}}$)**	
$\boldsymbol{K_{SEE}}$	**315.4 N/mm**	The stiffness of the SEE that resulted in the best match of model and experimental PF moment is consistent with values reported for the Achilles' tendon in the literature from both models (375.6 N/mm) [18] and experiments (188–805 N/mm) [26]–[28].

*Parameters are all defined in more detail within the text. **Bold** indicates a parameter set using optimization to match model and experimental data ($\vec{\boldsymbol{M}}$); un-bold indicates a parameter based on values taken from literature.

D. Inverse Approach to Simulate Walking with Ankle EXOs Over a Range of Stiffnesses

With the EXO component of the model defined and parameters of the lumped biological MTU set to $\vec{M}_{\rm bio}$, we sought to examine changes in mechanics and energetics of the biological MTU during walking with EXO springs ranging 0% to 100% of the MTU series elastic stiffness $K_{\rm SEE} = 315.4\,{\rm N/mm}$. This yielded equivalent EXO rotational stiffness values ranging from 0 N·m/rad (0 N·m/deg) up to 526.7 N·m/rad (9.19 N·m/deg), a value similar to that observed for the ankle joint in late stance during normal walking at 1.25 m/s [35].

For these simulations, we used an inverse approach [see Fig. 1(b)] that conserved ankle joint angle $\theta_{\rm ANKLE}$, and by extension, the lumped PF MTU length change $L_{\rm PF_{mtu}}$ (i.e.,

kinematics) as well as the *total* PF moment profile $m_{\mathrm{PF}_{\mathrm{total}}}$ (i.e., kinetics), generated by the $\vec{M}_{\mathrm{bio}}$ solution. First, F_{EXO} was calculated for each point in the stride according to (3) and then converted to m_{EXO}, assuming for simplicity that it followed the same line of action as the PFs by applying a moment arm computed from the model's skeletal geometry (∼4.1 cm on average). Next, we computed the moment generated by the biological MTUs, $m_{\mathrm{PF}_{\mathrm{mtu}}}$ (PFs) and $m_{DF_{\mathrm{mtu}}}$ (dorsiflexors) using

$$m_{\mathrm{PF}_{\mathrm{mtu}}}(t) = m_{\mathrm{PF}_{\mathrm{total}}}(t) - m_{\mathrm{EXO}}(t), \quad \text{where } m_{\mathrm{EXO}} < m_{\mathrm{PF}_{\mathrm{total}}} \tag{4}$$

and

$$m_{\mathrm{PF}_{\mathrm{mtu}}} = 0$$
$$m_{\mathrm{DF}_{\mathrm{mtu}}}(t) = m_{\mathrm{EXO}}(t) - m_{\mathrm{PF}_{\mathrm{total}}}(t), \quad \text{where } m_{\mathrm{EXO}} >= m_{\mathrm{PF}_{\mathrm{total}}}.$$

In cases where m_{EXO} was greater than $m_{\mathrm{PF}_{\mathrm{total}}}$ (i.e., $m_{\mathrm{PF}_{\mathrm{mtu}}} < 0$), we set $m_{\mathrm{PF}_{\mathrm{mtu}}} = 0$ and assumed that the excess EXO moment $(m_{\mathrm{EXO}} - m_{\mathrm{PF}_{\mathrm{total}}})$ would be compensated for by a moment from the antagonist muscle compartment (i.e., dorsiflexors) $m_{\mathrm{DF}_{\mathrm{mtu}}}$ to conserve the net ankle joint moment (see also Section II-E3).

Next, to get at the biological muscle–tendon dynamics, we converted $m_{\mathrm{PF}_{\mathrm{total}}}$ to $F_{\mathrm{PF}_{\mathrm{total}}}$, again using a moment arm computed from the model's skeletal geometry (∼4.1 cm on average). Given that all elements of the PF MTU are in series

$$F_{\mathrm{PF}_{\mathrm{mtu}}}(t) = F_{\mathrm{SEE}}(t) = F_{\mathrm{CE}}(t) \tag{5}$$

we could use $F_{\mathrm{SEE}}(t)$ (see (5)) and K_{SEE} to compute $L_{\mathrm{SEE}}(t)$ (see Equations S7, S8). $L_{\mathrm{SEE}}(t)$ was then subtracted from $L_{\mathrm{PF}_{\mathrm{mtu}}}(t)$ to determine the $L_{\mathrm{CE}}(t)$ profile (see Equation S9). With $L_{\mathrm{CE}}(t)$ defined for all points during the stride, we could compute a time derivative to obtain the muscle fascicle (CE) velocity $V_{\mathrm{CE}}(t)$. Finally, we could use our model for CE force to back calculate the muscle activation $\alpha(t)$ over the stride given the known $F_{\mathrm{CE}}(t)$, $L_{\mathrm{CE}}(t)$ and $V_{\mathrm{CE}}(t)$ (see Equation S1). At this point, the forces, lengths, and velocities of the EXO, MTU, SEE, and CE, as well as the activation of the CE were all known and available to assess the *muscle-level* mechanical and energetic performance of a given EXO stiffness during assisted walking.

E. Assessment Metrics for Quantifying EXO Performance at the Muscle Level

To evaluate the effects of different EXO springs on underlying PF mechanics and energetics, we calculated mechanical power of the MTU and its elements (CE and SEE) as well as the metabolic power of the CE.

1) Mechanical Power: For a given element (MTU, CE, or SEE), mechanical power (in watts) $P_{\mathrm{Mech}}(t)$ was calculated by taking the product of force and velocity at each time point over the stride

$$P_{\mathrm{Mech}}(t) = F_{\mathrm{element}}(t) * V_{\mathrm{element}}(t). \tag{6}$$

The total positive mechanical work (in joules) performed by each element over the stride was also calculated by integrating the mechanical power curves over the stride only in regions with $P_{\mathrm{Mech}} > 0$

$$W^{+}_{\mathrm{Mech}} = \int P^{+}_{\mathrm{Mech}}(t) * dt. \tag{7}$$

2) Metabolic Power: A mathematical model based on isolated muscle experiments was used to estimate the metabolic energy expenditure by the lumped PF muscles (CE) over the stride [36], [37] [see (8)–(11)]. The heat generated in each state of the muscle contraction, including maintenance, shortening, resting, and activation, are represented in this calculation. The metabolic power (in watts) $P_{\mathrm{Met}}(t)$ is given as

$$P_{\mathrm{Met}}(t) = \alpha(t) {}^{*} F_{\mathrm{CE}_{\mathrm{MAX}}} {}^{*} V_{\mathrm{CE}_{\mathrm{MAX}}} {}^{*} f_{\mathrm{met}}(\widetilde{V_{\mathrm{CE}}}(t)) \tag{8}$$

where $f_{\mathrm{met}}(\widetilde{V_{\mathrm{CE}}})$ represents empirically based heat measures that have been related to muscle velocity [36]

$$f_{\mathrm{met}}\left(\widetilde{V_{\mathrm{CE}}}(t)\right) = 0.23 - 0.16e^{-8\widetilde{V_{\mathrm{CE}}}}, \quad \widetilde{V_{\mathrm{CE}}} \geq 0 \tag{9}$$

$$f_{\mathrm{met}}\left(\widetilde{V_{\mathrm{CE}}}(t)\right) = 0.01 - 0.11\widetilde{V_{\mathrm{CE}}} + 0.06e^{23\widetilde{V_{\mathrm{CE}}}}, \ \widetilde{V_{\mathrm{CE}}} < 0. \tag{10}$$

Total metabolic work (in joules) expended over a stride was calculated by integrating the metabolic power curves

$$W_{\mathrm{Met}} = \int P_{\mathrm{Met}}(t) * dt. \tag{11}$$

3) Compensatory Metabolic Cost: A compensatory metabolic cost was also calculated for K_{EXO} values in which EXO forces/moments exceeded total PF forces/moments and resulted in a compensatory moment from the antagonist muscle compartment (i.e., dorsiflexors) $m_{\mathrm{DF}_{\mathrm{mtu}}}$ as per (4). First, we calculated the stride average metabolic cost per unit moment, *C* (in J/N·m) for the PFs in the $\vec{M}_{\mathrm{bio}}$ solution (i.e., the case with no EXO included)

$$C = \frac{\int P_{\mathrm{Met}}(t) * dt}{\int m_{\mathrm{PF}_{\mathrm{mtu}}}(t) * dt}. \tag{12}$$

Then, to compute the compensatory metabolic cost (in joules), we integrated and scaled the compensatory dorsiflexor moment $m_{\mathrm{DF}_{\mathrm{mtu}}}$ using the constant *C*

$$W_{\mathrm{MetComp}} = C * \int m_{\mathrm{DF}_{\mathrm{mtu}}}(t) * dt. \tag{13}$$

III. Results

EXOs with increasing stiffness developed higher and higher forces/moments over the period from ∼10% to 60% of the walking stride (see Fig. 2, top). Because the total EXO + biological PF moment was fixed in all conditions (i.e., invariant net ankle joint moment constraint), as the EXO contribution to the total moment increased, the moment generated by lumped PF muscle forces (CE) systematically decreased (see Fig. 2, bottom; Fig. 3). For the highest EXO stiffnesses (e.g., 0.9 K_{SEE}), the EXO moment greatly exceeded the lumped PF moment necessary to maintain an invariant net ankle moment, especially early in the stride cycle. In these cases, a compensatory moment from

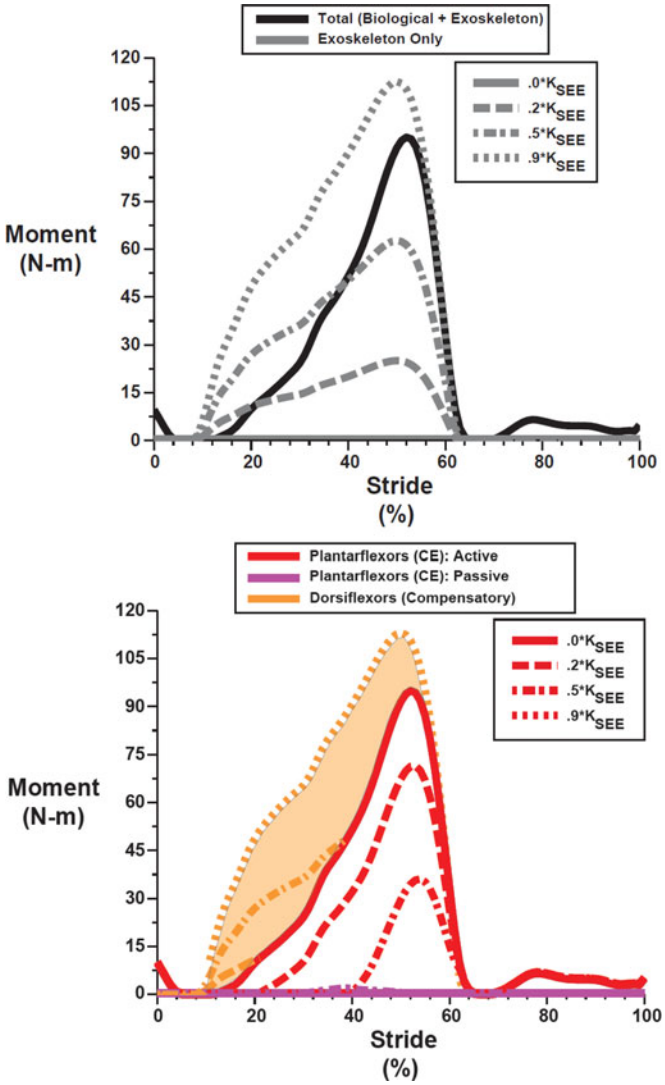

Fig. 2. Total contribution to ankle joint moment from the lumped PFs and the elastic ankle EXO (biological + EXO) (*Top*, black) and the moment generated by the EXO (EXO only) (*Top*, gray) over a walking stride from heel strike (0%) to heel strike (100%) for different EXO spring stiffnesses. The total moment is always the same because we constrained the model to follow the PF contribution to net ankle moment during unassisted walking (i.e., $\vec{M}_{\mathrm{bio}}$ solution) in *all* conditions. The active (*Bottom*, red) and passive (*Bottom*, purple) lumped PF muscle (CE) moment (i.e., biological only) for different EXO spring stiffnesses. For EXO springs $>0.2\ K_{\mathrm{SEE}}$, the EXO moment exceeds the total moment and necessitates a compensatory antagonist moment from dorsiflexors (*Bottom*, shaded area = difference between orange curves and solid red curve) to maintain an invariant net ankle moment. Curves are plotted for EXO stiffness values ranging from $0.2\ K_{\mathrm{SEE}}$ (~105 N·m/rad) to $0.9\ K_{\mathrm{SEE}}$ (~474 N·m/rad).

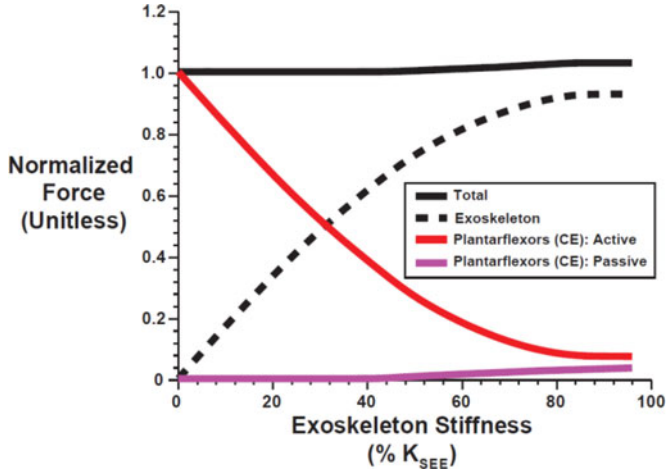

Fig. 3. Peak force versus EXO spring stiffness for the total = EXO + lumped PFs (solid black), EXO only (dashed black), and the active (solid red) and passive (solid purple) elements of the lumped PF muscles (CE). For each EXO stiffness, all forces are normalized to the peak total force (~3200 N) without an EXO. EXO spring stiffness of 100% K_{SEE} is equivalent to ~527 N·m/rad.

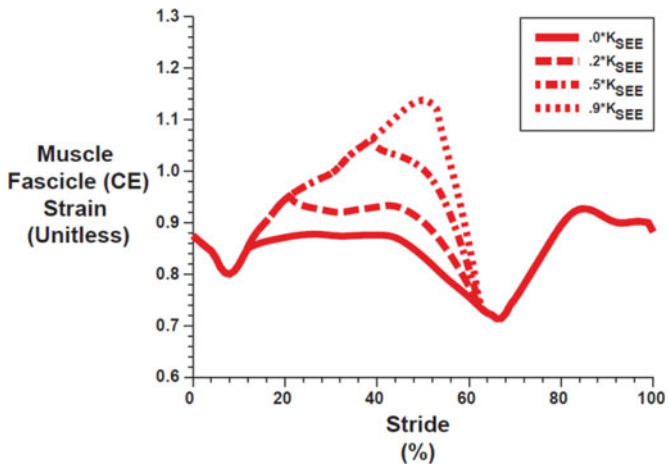

Fig. 4. Lumped PF muscle fascicle (CE) strain over a walking stride from heel strike (0%) to heel strike (100%) for different EXO spring stiffnesses. The solid red line is the fascicle strain pattern taken from Rubenson *et al.* [1] for $\vec{M}_{\mathrm{bio}}$ solution. Curves are plotted for EXO stiffness values ranging from 0.2 K_{SEE} (~105 N·m/rad) to 0.9 K_{SEE} (~474 N·m/rad).

antagonist muscles (e.g., dorsiflexors) was needed to maintain the net ankle force/moment from walking without an EXO (see Fig. 2, bottom). In addition, for stiffnesses above $\sim 0.5\ K_{\mathrm{SEE}}$ (263 N·m/rad), the lumped PF muscle (CE) produced some passive force/moment (see Fig. 2, bottom; Fig. 3).

Lumped PF muscle fascicles (CE) underwent larger excursions during stance phase (~10%–60% stride) with increasing EXO spring stiffness (see Fig. 4). Because the ankle joint angle profile was conserved across all conditions, increasing EXO forces served to reduce the force and strain in the SEE which, in turn, resulted in increased CE length changes (and CE velocities) with increasing EXO stiffness. In fact, L_{CE} surpassed L_{CE_0} (strain > 1.0) for $K_{\mathrm{EXO}} >\sim 0.5\, K_{\mathrm{SEE}}$, and resulted in passive force generation. CE strain values reached ~1.15 for the stiffest EXO springs.

As EXO spring stiffness (K_{EXO}) increased, mechanical power/work generated by the lumped PF MTU decreased linearly due to systematic decreases in biological forces/moments (see Fig. 5, top; Fig. 6). As expected, the power/work performed by the CE was approximately equal in magnitude to the power/work performed by the SEE for the condition without an EXO. As K_{EXO} increased, the mechanical power/work generated by the muscle fascicles (CE) and series elastic tissues (SEE) both decreased, but the SEE well outpaced the CE leaving the CE as the dominant contributor to overall MTU

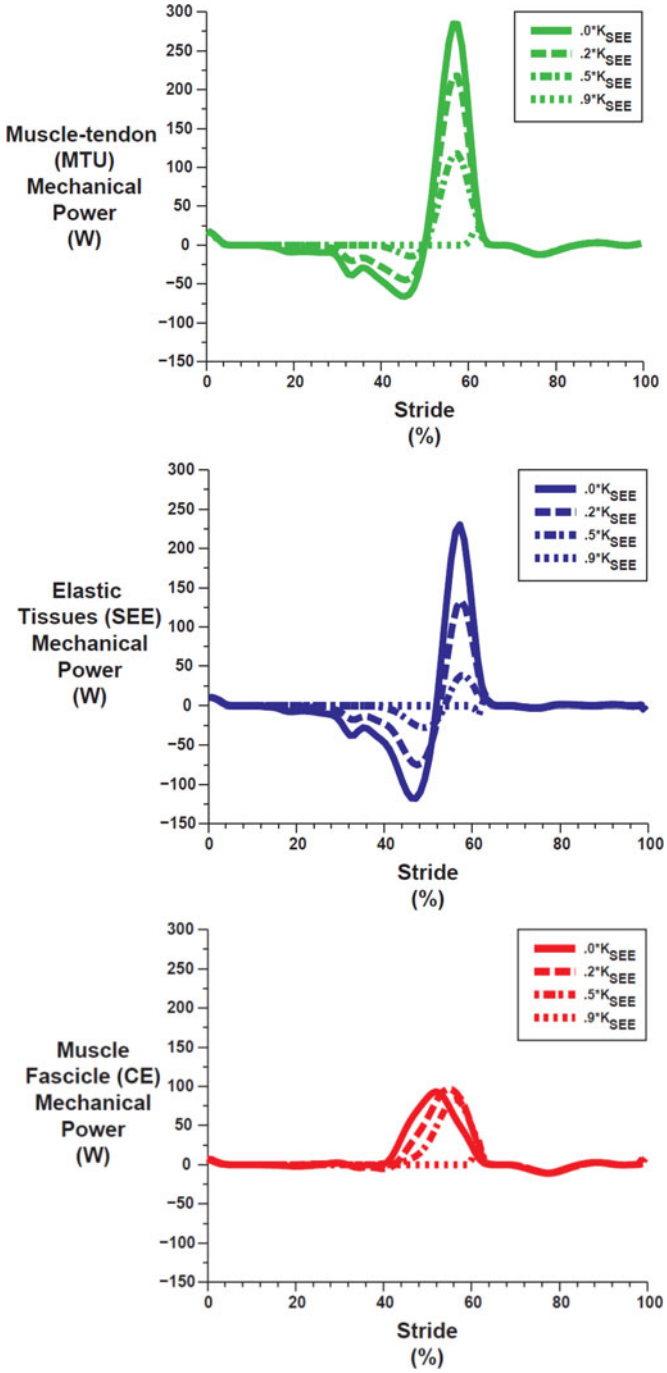

Fig. 5. Mechanical power over a walking stride from heel strike (0%) to heel strike (100%) for the lumped PF MTU (*Top*, green); elastic tissues (SEE) (*Middle*, blue) and muscle fascicles (CE) (*Bottom*, red). Curves with varying line types represent different EXO stiffness values ranging from no EXO (bold) up 0.9 K_{SEE} (∼474 N·m/rad).

power/work for EXOs with $K_{\mathrm{EXO}} >\sim 0.1\,K_{\mathrm{SEE}}$ (see Fig. 6). In fact, CE power/work did not decrease for $K_{\mathrm{EXO}} <\sim 0.2\,K_{\mathrm{EXO}}$ (∼105 N·m/rad), as reduced CE forces traded-off with increased CE velocities/excursions (see Fig. 4) keeping CE power/work relatively constant. For $K_{\mathrm{EXO}} > 0.2$, reductions in force began to dominate the increases in velocity and CE power/work began to sharply decline (see Fig. 6).

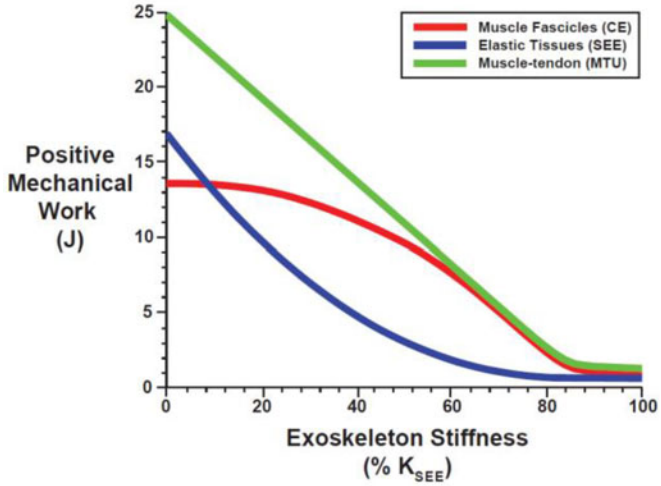

Fig. 6. Positive mechanical work versus EXO spring stiffness for the lumped PF muscle fascicles (CE) (red), elastic tissues (SEE) (blue), and MTU (green). EXO spring stiffness of 100% K_{SEE} is equivalent to ∼527 N·m/rad.

Lumped PF muscle (CE) activation and metabolic power/work both decreased with increasing EXO stiffness (K_{EXO}) (see Fig. 7). Metabolic cost decreased more slowly than muscle activation with increasing EXO stiffness (see Fig. 7, bottom left) because the higher CE velocities associated with stiffer EXO springs required more activation to achieve similar force levels. That is, with higher EXO spring stiffness, CE force/unit activation decreases due to unfavorable force–velocity effects. Although increasing K_{EXO} sharply reduced the metabolic cost of the lumped PFs, the metabolic cost of compensatory forces/moments needed to maintain an invariant net ankle moment sharply increased with increasing K_{EXO} (see Fig. 7, bottom right). As a result, the total metabolic cost had a minimum at $K_{\mathrm{EXO}} =\sim 0.7\,K_{\mathrm{EXO}}$ (∼369 N·m/rad) and was ∼30% lower than the cost of ankle muscle activity for normal walking without EXOs.

IV. Discussion

The goal of this study was to employ a strategically simple musculoskeletal model of an elastic ankle EXO working in parallel with the biological PFs to determine how EXO stiffness would influence the neuromechanics and energetics of the underlying MTUs during walking. We hypothesized that increasing EXO stiffness would result in (1) increased unloading of biological muscle–tendons and larger reductions in the metabolic cost of the PFs during walking. Furthermore, we surmised that if EXOs got *too* stiff, (2) costly compensations might arise in other muscles in order to maintain steady-gait mechanics. Finally, at the muscle–tendon level, we hypothesized that (3) despite lower biological force/moment requirements due to EXO assistance, it was possible that the unfavorable changes in muscle operating length and/or higher muscle shortening velocities due to a disrupted "catapult mechanism" early in the stance phase of the stride could increase metabolic energy requirements in the PF muscles and offset some of the potential benefit of increased assistance from elastic ankle EXOs. Our modeling results

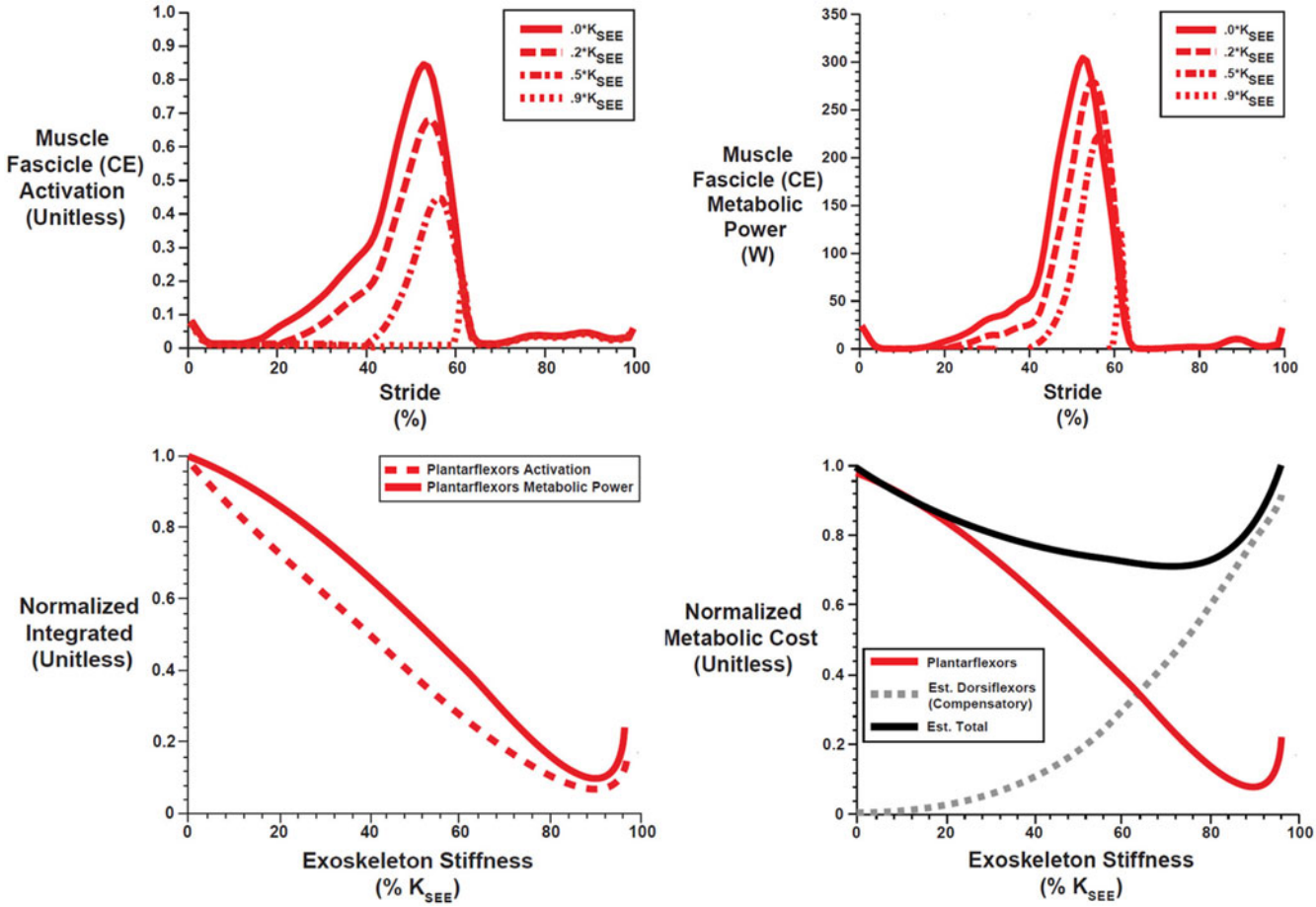

Fig. 7. (*Top*) Lumped PF muscle fascicle (CE) activation (*Top left*) and metabolic power (*Top right*) over a walking stride from heel strike (0%) to heel strike (100%) for different EXO spring stiffnesses. The solid red lines represent walking without an EXO (i.e., the $\vec{M}_{\rm bio}$ solution). Curves of varying line type represent EXO stiffness values ranging from 0.2 $K_{\rm SEE}$ ($\sim$105 N·m/rad) to 0.9 $K_{\rm SEE}$ ($\sim$474 N·m/rad). (*Bottom*) Integrated activation (*Left*, dashed) and metabolic power (i.e., work) (*Left*, solid) versus EXO spring stiffness for the lumped PF muscle fascicles (CE). Integrated metabolic power (*Right*, red) is modified (*Right*, black) to include an estimated compensatory metabolic cost (*Right*, dashed gray) due to the antagonist dorsiflexor muscle moment required to maintain an invariant net ankle moment. All values are normalized to the no EXO condition. EXO spring stiffness of 100% $K_{\rm SEE}$ is equivalent to $\sim$527 N·m/rad.

support all of these hypotheses and suggest potential muscle-level mechanisms behind the recently observed "sweet spot" in elastic ankle EXO stiffness [25] that must now be confirmed with follow-up experiments using ultrasound imaging.

As expected, stiffer ankle EXO springs resulted in larger decreases in PF metabolic energy consumption. Humans seem to employ a motor control strategy in order to maintain relatively invariant net ankle joint moments during locomotion with mechanical assistance from ankle exoskeletal devices [10]–[12], [15], [20], [25], [29], [30]. To capture the phenomenon of kinetic invariance in humans, we employed a modeling framework that enforced both the ankle angle and PF contribution to net ankle joint moment using experimental data from normal walking at 1.25 m/s. Not surprisingly, solutions with kinetic invariance demonstrated that increasing $K_{\rm EXO}$ yields a clear tradeoff between EXO and biological muscle forces, with a $\sim$50/50% sharing at $K_{\rm EXO} =\sim 0.3\, K_{\rm SEE}$ ($\sim$158 N·m/rad = 2.8 N·m/deg) (see Fig. 3). In addition, solutions with higher $K_{\rm EXO}$ required muscle activation with lesser magnitude *and* later onset (see Fig. 7, top left), a result consistent with recent experimental data showing decreases in soleus activity that are more pronounced with higher EXO springs stiffness [25]. We note, without this timing shift, the lumped PF muscles (CE) would have produced unnecessary forces/moments between $\sim$10% and 60% of the stride when EXO assistance $m_{\rm EXO}$ was already sufficient (see Fig. 2). Thus, in line with our hypothesis (1), as the biological force/moment requirement declined with increasing $K_{\rm EXO}$, so did muscle activation, which was the main driver of metabolic cost (see Fig. 7),

Metabolic cost of the PFs reached a minimum value of $\sim$11% of the value during unassisted walking (50.3 J $*$ 0.11 = 5.5 J per leg) with a $K_{\rm EXO}$ of $\sim$0.8 $K_{\rm SEE}$ ($\sim$421 N·m/rad = 7.4 N·m/deg) (see Fig. 7, bottom right). But, is more necessarily better when it comes to ankle EXO stiffness selection [25], [33], [38]? Interestingly, in our model, assisting with a $K_{\rm EXO} \geq\sim 0.5\, K_{\rm SEE}$ (263 N·m/rad) began to induce passive stretch in the muscle fascicles (CE) and, thus, a passive muscle moment contribution. While relying more on passive contributions to muscle force could have metabolic benefit, it also elicits an unavoidable deviation in the ankle force/moment profile from normal walking

(see Figs. 2 and 3). Thus, due to shifts in the operating point of underlying muscles to longer lengths (see Fig. 4), perfectly conserving the $m_{\mathrm{PF}_{\mathrm{total}}}$ may become increasingly difficult, and could be a factor that limits performance for EXOs employing high parallel stiffness [11], [25], [31].

If humans choose to move with very strict ankle moment invariance, our model suggests that they may reject EXOs with stiffness $\geq 0.5\ K_{\mathrm{SEE}}$ (or $\sim$50–60% of normal ankle joint rotational stiffness during walking at 1.25 m/s [35]), where passive forces in PFs are unavoidable. This could severely limit the potential for metabolic savings to only $\sim$60% of the total PF contribution or $\sim$15% overall [39]. Solutions with $K_{\mathrm{EXO}} \geq 0.5\,K_{\mathrm{SEE}}$ (263 N·m/rad) begin to significantly produce excess EXO forces/moments early in the stance phase (see Fig. 2). To maintain net ankle moment invariance, these excess moments would need to be countered by significant antagonist moments coming from ankle dorsiflexors or adjustments in posture, both of which would likely incur a compensatory metabolic cost (see Fig. 7, lower right). Thus, a 15% reduction in overall metabolic cost of walking seems a high end estimate.

Interestingly, when adding in our estimate for the metabolic cost of compensatory force/moment of ankle antagonists (i.e., dorsiflexors), our model predicts a broad "sweet spot" between $K_{\mathrm{EXO}} = 0.6$ and $0.8\ K_{\mathrm{SEE}}$ ($\sim$316–420 N·m/rad) with a net metabolic benefit of $\sim$30% for the ankle PFs. Using Umberger's estimate that PFs account for $\sim$27% of the total metabolic cost of walking [39], [40], this is equivalent to an overall reduction in the metabolic cost of walking of $\sim$8% and falls very near to the measured value of Collins *et al.* [25], albeit at a higher range of EXO stiffness. Collins *et al.* found the "sweet spot" at 180 N·m/rad, about half the stiffness for the metabolic minimum reported here. The mismatch is likely due to the very rudimentary approach we took to the compensatory metabolic cost in this study, which assumed dorsiflexors and PFs have the same metabolic cost per unit moment [C in (13)] and did not account for the metabolic cost of compensation elsewhere in the body (e.g., increased knee flexor moments).

Despite the mismatch in the "sweet spot" stiffness between our model and experiments, our results still lend some support to hypothesis (2) that metabolically costly compensation may be at play to maintain invariant net ankle moment in the face of increasing EXO spring stiffness, an idea that is also corroborated by data from Collins *et al.* [25] indicating both local and global neuromechanical compensations during walking with parallel springs. At the ankle, compensation appears as elevated tibialis anterior muscle activity in early stance and late swing. More globally, increased knee joint moments appear near the stance-swing transition—an effect not captured by the current model.

Despite the potential for significant metabolic savings due to reduced muscle forces and activations (see Figs. 2, 3, and 7), our results also support hypothesis (3) that elastic ankle EXOs could significantly disrupt the normal "catapult action" of the PFs during human walking. Our model of normal walking at 1.25 m/s (i.e., $K_{\mathrm{EXO}} = 0$) captures the normal muscle–tendon interaction dynamics of the PFs and Achilles' tendon during walking with nearly isometric muscle fascicles during stance phase (see Fig. 4, bold red) and large amounts of elastic energy storage and return in series elastic tissues (see Fig. 5, middle, bold blue) [22], [41]. This results in a large burst of mechanical power at push-off that is shared $\sim$50/50 between muscle fascicles (CE) and series elastic tissues (SEE) (see Figs. 5 and 6) [22]. However, as K_{EXO} increases, unloading of the biological MTU causes less and less stretch in the SEE and more and more stretch in the CE, disrupting the normal "catapult-like" muscle–tendon interaction (see Figs. 4–6).

The observation of larger CE excursions with parallel mechanical assistance is consistent with recent muscle-level experiments during spring-loaded human hopping. Soleus fascicles undergo increased excursions in the presence of a parallel spring ($K_{\mathrm{EXO}} = 91\,\mathrm{N \cdot m/rad}$) providing assistive PF torque [20]. In that case, reduced forces were counteracted by increased length changes resulting in no difference in soleus muscle fascicle work between spring-loaded and unassisted hopping conditions. Our model of spring-loaded walking makes a similar prediction that CE work does not decrease for values of K_{EXO} up to $\sim 0.2\ K_{\mathrm{SEE}}$ ($\sim$ 105 N·m/rad = 1.8 N·m/deg) (see Fig. 6). For EXO stiffness values $> 0.2\,K_{\mathrm{SEE}}$, CE work begins to decline as reductions in muscle force outpace increases in CE length changes. Perhaps more striking is the rapid reduction in the mechanical work performed by the SEE recoil with increasing EXO spring stiffness. Without assistance from the EXO, the SEE recoil contributes an equal amount of mechanical power as CE shortening, but the SEE contribution is reduced to nearly zero for $K_{\mathrm{EXO}} \geq 0.7\,K_{\mathrm{SEE}}$ ($\sim$369 N·m/rad), completely eliminating the ability of the biological MTU to function as a catapult (see Fig. 6).

Increasing reliance on the CE for MTU power production limits the metabolic benefit of increasing EXO spring stiffness. The lack of mechanical power from elastic recoil of the SEE is mostly supplanted by elastic recoil of the EXO spring, but not without some consequence. Our metabolic cost model is driven by muscle activation, force–length, and force–velocity dynamics [36] [see (8)–(11)]. As EXO spring stiffness increases, the required muscle activation declines because biological muscle force requirements are reduced. We note, however, that for the stiffest EXOs, reductions in metabolic cost occur at a slower rate than reductions in muscle activation (see Fig. 7, bottom left). This is a direct side effect of the metabolic penalty associated with higher CE shortening velocities due to the increased muscle excursions characteristic of a disrupted "catapult action" (see Fig. 4). Interestingly, because muscle fascicles nominally operate down the ascending limb (see Fig. 4, red bold curve), EXO assistance tends to increase average fascicle lengths toward $L_{\mathrm{CE}o}$, an operating point that is more favorable for force production—an effect that is trumped by far less favorable force–velocity operating points. Thus, in general, it would seem that EXOs designed to assist MTUs with compliant architecture may be inherently limited in their metabolic benefit. One way out of this conundrum might be for the user to adjust their joint kinematics (and, therefore, MTU length change pattern) in order to attenuate increases in underlying fascicle velocity that counteract the metabolic reductions due to reduced muscle forces and activations [20]. Indeed, altered joint kinematics indicative of shorter MTU lengths (i.e., exaggerated plantarflexion) have

been observed during walking with powered ankle orthoses [2], [29], [30]—a strategy that may limit metabolic penalty due to a disrupted "catapult mechanism."

Aside from improving metabolic performance of the user, exaggerated plantar flexion during walking with an ankle EXO could be indicative of an injury avoidance mechanism. Although nonintuitive, walking with relatively stiff EXO springs could induce passive stretch at high rates in the CE and increase the likelihood of a muscle strain injury [42]. In our simulations, the CE strain reached maximum values of $\sim$115% for the stiffest EXO spring (see Fig. 4), but for tasks where the MTU operates at longer lengths and/or faster velocities (e.g., faster walking or walking uphill), it is possible that strains/strain rates might reach dangerous levels with relatively stiff EXOs (e.g., $K_{\mathrm{EXO}} > 0.9\% \, K_{\mathrm{SEE}} = 475\,\mathrm{N} \cdot \mathrm{m/rad}$).

A. Model Limitations

We made a number of simplifications and assumptions in developing the model and simulations used in this study that are worth addressing. First and foremost, we greatly simplified the attachment geometry, muscle–tendon architecture, and mechanisms driving force production in our musculoskeletal model of the triceps surae [i.e., medial gastrocnemius (MG), lateral gastrocnemius (LG) and soleus (SOL)]. Briefly, we combined the triceps surae group into a single, "lumped" uniarticular muscle–tendon with a soleus like origin and insertion locations, but with a force generating capacity of the summed MG + LG + SOL. Despite its simplicity, we believe that the model captures the salient features and behaviors exhibited by the human PFs during walking that are relevant to the questions we address in this study.

The inverse modeling framework we employed assumed that the overall ankle joint kinematics *and* kinetics during walking at 1.25 m/s remain invariant in the context of elastic ankle EXOs. While there is strong evidence that humans do indeed exhibit invariance in ankle joint moments during walking [11], [25], [29], [30], the evidence for ankle joint angle invariance is weaker. For example, Kao *et al.* demonstrated that while ankle kinetics are conserved when some PF moment is provided by a robotic EXO, ankle kinematics tend to shift to more plantarflexed postures [29]. This finding has been corroborated by others who use ankle EXOs during human walking studies [2], [30]. We note that it is entirely possible that the devices used in previous studies were not properly "tuned" to reproduce both ankle kinetics and kinematics during the studied gait pattern. In fact, our study strongly suggests that assistive devices that are not properly "tuned" could lead to deviations from normal moments (see Fig. 3) unless the user significantly adjusts their joint kinematics and/or muscle activation patterns (see Fig. 7).

On the other hand, it may be that the conditions we simulated, maintaining kinematic and kinetic invariance, are not the best strategy for minimizing the metabolic cost. A gait pattern with more plantarflexed posture or a higher total net PF moment may be able to better optimize the tradeoff between the energy savings from reduced PF forces/muscle activations and the additional energy costs of altered movement at other places in the body (e.g., knee or hip).

To address these open questions, our future work will aim toward a more complete model with more detailed anatomy and physiology that incorporates all of the individual ankle joint muscle–tendons and the rest of the lower limb as along with an elastic ankle EXO (e.g., [32] for hopping) during human waking. We will use our inverse framework, but drive the simulations with actual kinematic and kinetic data from walking with elastic EXOs with varying spring stiffness (e.g., [25]) rather than imposing invariant constraints as we did in this study. Comparing and contrasting the fully constrained model presented here, with a model driven by "real-world" EXO walking data will provide important insights into the muscle-level mechanisms that may be guiding human preference during locomotion with EXO assistance. We also plan to use ultrasound imaging to verify the model predictions of underlying fascicle behavior during EXO-assisted walking. Indeed, a grand challenge in the field of wearable robotics is to develop a modeling and simulation framework that does not rely at *all* on imposed kinematic or kinetic constraints (from data or otherwise) to predict how walking mechanics and energetics would change in the context of novel devices.

B. Insights Into Improving Current Ankle EXO Designs

In this study, we have highlighted a number of limitations inherent in passive elastic EXO designs [8], [24] that may be overcome with improvements in future designs. The primary drawback to the device we simulated was that it produced forces too early in the stance phase that often exceeded those needed to produce a normal ankle joint moment. This effect was particularly noticeable as the EXO spring stiffness increased (see Figs. 2 and 3). With the current design, avoiding this excess EXO moment would require either 1) a change in ankle joint kinematics, or 2) coactivation by ankle dorsiflexors to adjust the net ankle moment downward, or 3) walking with excessive total ankle joint moments—all of which could be considered undesirable effects. Changes in the EXO design could also improve performance. For example, a passive device with nonlinear spring stiffness (i.e., a stiffening spring), and/or a changing moment arm could be designed with a custom torque angle curve appropriate for a given gait. In addition, timing engagement of the spring with a more versatile clutching mechanism could provide flexibility in when the EXO torque onset occurs during a gait cycle. Of course, a device with motors could achieve all of the aforementioned performance features by employing customized gait-phase-dependent torque control that is optimized to maximize metabolic benefit while maintaining joint kinetics and kinematics.

V. Conclusion

Our modeling results and recent experimental evidence [25] both indicate that for devices intended to reduce the metabolic cost of human locomotion by assisting compliant joints (e.g., ankle), the name of the game is to reduce muscle forces and activations. This idea represents somewhat of a paradigm shift from previous solutions focusing on reducing biological muscle-tendon/joint positive mechanical power outputs [30], [43], [44], especially in late stance phase. Passive elastic solutions are a

promising alternative as they are well suited for reducing muscle force and activation requirements in parallel biological MTUs even during periods of energy absorption [25].

ACKNOWLEDGMENT

The authors would like to thank G. Lichtwark and J. Rubenson for helpful discussions regarding the choice of model parameters, and S. Collins for crucial feedback on the approach.

REFERENCES

[1] J. Rubenson *et al.*, "On the ascent: The soleus operating length is conserved to the ascending limb of the force-length curve across gait mechanics in humans," *J. Exp. Biol.*, vol. 215, no. Pt 20, pp. 3539–3551, Oct. 15, 2012.

[2] G. S. Sawicki and D. P. Ferris, "Mechanics and energetics of level walking with powered ankle exoskeletons," *J. Exp. Biol.*, vol. 211, no. Pt 9, pp. 1402–1413, May 2008.

[3] S. R. Ward *et al.*, "Are current measurements of lower extremity muscle architecture accurate?" *Clin. Orthopaedics Relat. Res.*, vol. 467, no. 4, pp. 1074–1082, Apr. 2009.

[4] H. Geyer *et al.*, "Compliant leg behaviour explains basic dynamics of walking and running," *Proc. Biol. Sci.*, vol. 273, no. 1603, pp. 2861–2867, Nov. 22, 2006.

[5] C. T. Farley *et al.*, "Hopping frequency in humans: A test of how springs set stride frequency in bouncing gaits," *J. Appl. Physiol.*, vol. 71, no. 6, pp. 2127–2132, Dec. 1991.

[6] R. Blickhan, "The spring-mass model for running and hopping," *J. Biomech.*, vol. 22, nos. 11/12, pp. 1217–1227, 1989.

[7] T. J. Roberts and E. Azizi, "Flexible mechanisms: The diverse roles of biological springs in vertebrate movement," *J. Exp. Biol.*, vol. 214, no. Pt 3, pp. 353–361, Feb. 1, 2011.

[8] M. B. Wiggin *et al.*, "An exoskeleton using controlled energy storage and release to aid ankle propulsion," presented at the IEEE Int. Conf. Rehabilitation Robotics, Zurich Switzerland, 2011, vol. 2011, p. 5975342.

[9] A. M. Grabowski and H. M. Herr, "Leg exoskeleton reduces the metabolic cost of human hopping," *J Appl. Physiol.*, vol. 107, no. 3, pp. 670–678, Sep. 2009.

[10] D. J. Farris and G. S. Sawicki, "Linking the mechanics and energetics of hopping with elastic ankle exoskeletons," *J Appl. Physiol.*, vol. 113, no. 12, pp. 1862–1872, Dec. 15, 2012.

[11] D. J. Bregman *et al.*, "Spring-like ankle foot orthoses reduce the energy cost of walking by taking over ankle work," *Gait Posture*, vol. 35, no. 1, pp. 148–153, Jan, 2012.

[12] D. P. Ferris *et al.*, "Neuromechanical adaptation to hopping with an elastic ankle-foot orthosis," *J Appl. Physiol.*, vol. 100, no. 1, pp. 163–170, Jan. 2006.

[13] G. Elliott *et al.*, "The biomechanics and energetics of human running using an elastic knee exoskeleton," presented at the IEEE Int. Conf. Rehabilitation Robotics, Seattle, WA, USA, Jun. 2013, vol. 2013, p. 6650418.

[14] M. S. Cherry *et al.*, "Design and fabrication of an elastic knee orthosis: Preliminary results," in *Proc. 30th Annu. Mech. Robot. Conf.*, 2006, pp. 565–573.

[15] Y. H. Chang *et al.*, "Intralimb compensation strategy depends on the nature of joint perturbation in human hopping," *J. Biomech.*, vol. 41, no. 9, pp. 1832–1839, 2008.

[16] E. M. Arnold *et al.*, "A model of the lower limb for analysis of human movement," *Ann. Biomed. Eng.*, vol. 38, no. 2, pp. 269–279, Feb. 2010.

[17] G. A. Lichtwark and A. M. Wilson, "Is achilles tendon compliance optimised for maximum muscle efficiency during locomotion?" *J. Biomech.*, vol. 40, no. 8, pp. 1768–1775, 2007.

[18] P. Krishnaswamy *et al.*, "Human leg model predicts ankle muscle-tendon morphology, state, roles and energetics in walking," *PLoS Comput. Biol.*, vol. 7, no. 3, art. no. e1001107 (16 pages), Mar. 2011.

[19] H. Geyer and H. Herr, "A muscle-reflex model that encodes principles of legged mechanics produces human walking dynamics and muscle activities," *IEEE Trans. Neural Syst. Rehabil. Eng.*, vol. 18, no. 3, pp. 263–273, Jun. 2010.

[20] D. J. Farris *et al.*, "Elastic ankle exoskeletons reduce soleus muscle force but not work in human hopping," *J. Appl. Physiol.*, vol. 115, no. 5, pp. 579–585, Sep. 1, 2013.

[21] D. J. Farris and G. S. Sawicki, "The mechanics and energetics of human walking and running: A joint level perspective," *J. Roy. Soc. Interface*, vol. 9, no. 66, pp. 110–118, Jan. 7, 2012.

[22] D. J. Farris and G. S. Sawicki, "Human medial gastrocnemius force-velocity behavior shifts with locomotion speed and gait," *Proc. Nat. Acad. Sci. USA*, vol. 109, no. 3, pp. 977–982, Jan. 17, 2012.

[23] J. S. Gottschall and R. Kram, "Energy cost and muscular activity required for propulsion during walking," *J. Appl. Physiol.*, vol. 94, no. 5, pp. 1766–1772, May 2003.

[24] M. B. Wiggin *et al.*, "Apparatus and clutch for using controlled storage and release of mechanical energy to aid locomotion," U.S. Patent 20 130 046 218, Feb. 21, 2013.

[25] S. H. Collins *et al.*, "Reducing the energy cost of human walking using an unpowered exoskeleton," *Nature*, vol. 522, no. 7555, pp. 212–215, Jun. 11, 2015.

[26] G. A. Lichtwark and A. M. Wilson, "In vivo mechanical properties of the human Achilles tendon during one-legged hopping," *J. Exp. Biol.*, vol. 208, no. Pt 24, pp. 4715–4725, Dec. 2005.

[27] K. Albracht and A. Arampatzis, "Exercise-induced changes in triceps surae tendon stiffness and muscle strength affect running economy in humans," *Eur. J. Appl. Physiol.*, vol. 113, no. 6, pp. 1605–1615, Jun. 2013.

[28] L. Houghton *et al.*, "Achilles tendon mechanical properties after both prolonged continuous running and prolonged intermittent shuttle running in cricket batting," *J. Appl. Biomech.*, vol. 29, no. 4, pp. 453–462, Aug. 2013.

[29] P. C. Kao *et al.*, "Invariant ankle moment patterns when walking with and without a robotic ankle exoskeleton," *J. Biomech.*, vol. 43, no. 2, pp. 203–209, Jan. 19, 2010.

[30] P. Malcolm *et al.*, "A simple exoskeleton that assists plantarflexion can reduce the metabolic cost of human walking," *PLoS One*, vol. 8, no. 2, art. no e56137 (7 pages), 2013.

[31] D. J. Bregman *et al.*, "The effect of ankle foot orthosis stiffness on the energy cost of walking: A simulation study," *Clin. Biomech. (Bristol, Avon)*, vol. 26, no. 9, pp. 955–961, Nov. 2011.

[32] D. J. Farris *et al.*, "Musculoskeletal modelling deconstructs the paradoxical effects of elastic ankle exoskeletons on plantar-flexor mechanics and energetics during hopping," *J. Exp. Biol.*, vol. 217, pp. 4018–4028, Oct. 2, 2014.

[33] B. D. Robertson, D. J. Farris, and G. S. Sawicki, "More is not always better: Modeling the effects of elastic exoskeleton compliance on underlying ankle muscle-tendon dynamics," *Bioinspir. Biomim.*, vol. 9, no. 4, art. no. 046018 (11 pages), Dec. 2014.

[34] F. E. Zajac, "Muscle and tendon: Properties, models, scaling, and application to biomechanics and motor control," *Crit. Rev. Biomed. Eng.*, vol. 17, no. 4, pp. 359–411, 1989.

[35] K. Shamaei *et al.*, "Estimation of quasi-stiffness and propulsive work of the human ankle in the stance phase of walking," *PLoS One*, vol. 8, no. 3, art. no. e59935 (12 pages), 2013.

[36] R. M. Alexander, "Optimum muscle design for oscillatory movements," *J. Theor. Biol.*, vol. 184, no. 3, pp. 253–259, Feb. 7, 1997.

[37] A. E. Minetti and R. M. Alexander, "A theory of metabolic costs for bipedal gaits," *J. Theor. Biol.*, vol. 186, no. 4, pp. 467–476, Jun. 21, 1997.

[38] B. D. Robertson and G. S. Sawicki, "Exploiting elasticity: Modeling the influence of neural control on mechanics and energetics of ankle muscle-tendons during human hopping," *J. Theor. Biol.*, vol. 353, pp. 121–132, Jul. 21, 2014.

[39] B. R. Umberger and J. Rubenson, "Understanding muscle energetics in locomotion: New modeling and experimental approaches," *Exercise Sport Sci. Rev.*, vol. 39, no. 2, pp. 59–67, Apr. 2011.

[40] B. R. Umberger, "Stance and swing phase costs in human walking," *J. Roy. Soc. Interface*, vol. 7, no. 50, pp. 1329–1340, Sep. 6, 2010.

[41] M. Ishikawa *et al.*, "Muscle-tendon interaction elastic energy usage human walking," *J. Appl. Physiol.*, vol. 99, pp. 603–608, 2005.

[42] W. E. Garrett, Jr., "Muscle strain injuries: Clinical and basic aspects," *Med. Sci. Sports Exercise*, vol. 22, no. 4, pp. 436–443, Aug. 1990.

[43] L. M. Mooney *et al.*, "Autonomous exoskeleton reduces metabolic cost of human walking," *J. Neuroeng. Rehabil.*, vol. 11, art. no. 151 (5 pages), 2014.

[44] G. S. Sawicki *et al.*, "It pays to have a spring in your step," *Exercise Sport Sci. Rev.*, vol. 37, no. 3, pp. 130–138, Jul. 2009.

Authors' photographs and biographies not available at the time of publication.